Molecular Cancer Research

miR-155 Overexpression Promotes Genomic Instability by Reducing High-fidelity Polymerase Delta Expression and Activating Error-Prone DSB Repair

Jennifer R. Czochor[1], Parker Sulkowski[1], and Peter M. Glazer[1,2]

Abstract

miR-155 is an oncogenic miRNA that is often overexpressed in cancer and is associated with poor prognosis. miR-155 can target several DNA repair factors, including RAD51, MLH1, and MSH6, and its overexpression results in an increased mutation frequency *in vitro*, although the mechanism has yet to be fully understood. Here, we demonstrate that overexpression of miR-155 drives an increased mutation frequency both *in vitro* and *in vivo*, promoting genomic instability by affecting multiple DNA repair pathways. miR-155 overexpression causes a decrease in homologous recombination, but yields a concurrent increase in the error-prone nonhomologous end-joining pathway. Despite repressing established targets MLH1 and MSH6, the identified mutation pattern upon miR-155 overexpression does not resemble that of a mismatch repair–deficient background. Further investigation revealed that all four subunits of polymerase delta, a high-fidelity DNA replication, and repair polymerase are downregulated at the mRNA level in the context of miR-155 overexpression. FOXO3a, a transcription factor and known target of miR-155, has one or more putative binding site(s) in the promoter of all four polymerase delta subunits. Finally, suppression of FOXO3a by miR-155 or by siRNA knockdown is sufficient to repress the expression of the catalytic subunit of polymerase delta, POLD1, at the protein level, indicating that FOXO3a contributes to the regulation of polymerase delta levels.

Implications: Taken together, miR-155 overexpression drives an increase in mutation frequency via multifaceted impact on DNA damage response and DNA repair pathways. *Mol Cancer Res; 14(4); 363–73. ©2016 AACR.*

Introduction

MiRNAs have been described as master regulators of the genome. As such, their expression is tightly controlled in normal tissues. MiRNAs bind to mRNA transcripts of target genes and promote translational repression. Cancer cells often hijack these translational regulators by modifying their expression to promote cell survival and tumorigenesis. Understanding the mechanism and function behind misregulated miRNAs will provide insight into the potential adjuvant manipulation of these RNA mediators to improve targeted cancer therapies.

It has been shown that several factors can influence the regulation of miRNA expression, most notably aspects of the tumor microenvironment, such as hypoxia and inflammation. These environmental changes employ transcription factors to aberrantly modulate gene expression and promote cell survival. Overexpression of several miRNAs has been observed in response to hypoxia, ultimately resulting in facilitation of hypoxic hallmarks, such as therapy resistance, genomic instability, and the metabolic shift to glycolysis. One such miRNA, miR-155, is induced by hypoxia and subsequently promotes resistance to radiotherapy (1, 2).

miR-155 has been described as an oncomiR, an oncogenic miRNA, in part due to its association with poor prognosis in a variety of cancer types (3–5). miR-155 overexpression was initially identified in B-cell lymphoma, but has since been associated with several other malignancies, including lung, breast, and colon cancer (4–8). Recently, it was demonstrated that miR-155 overexpression alone was sufficient to drive lymphoma in a mouse model (9). Supporting its designation as an oncomiR, miR-155 has many tumor suppressor gene targets, including proapoptotic factors FOXO3a and TP53INP1 and negative regulators of proliferation SOCS1 and SHIP1 (10–13). Further evidence suggests that miR-155 is also responsible for targeting several genes essential for maintaining genomic integrity, including DNA repair factors MLH1 and RAD51 (14, 15). The essential nature of these and many other miR-155 targets emphasizes the importance of tight miR-155 regulation in maintaining cellular homeostasis and inhibiting tumorigenesis.

DNA repair is fundamental to the maintenance of genomic integrity. Although both single and double-strand breaks (DSB) are disruptive, DSBs are more toxic to a cell due to their propensity for genomic instability and cell death. DSB repair consists of two main pathways, nonhomologous end-joining (NHEJ) and homologous recombination (HR). Although these pathways work in concert with one another, NHEJ is the more frequently

[1]Department of Genetics, Yale University, New Haven, Connecticut. [2]Department of Therapeutic Radiology, Yale University, New Haven, Connecticut.

Note: Supplementary data for this article are available at Molecular Cancer Research Online (http://mcr.aacrjournals.org/).

Corresponding Author: Peter M. Glazer, Yale University, 333 Cedar Street, P.O. Box 208040, New Haven, CT 06520-8040. Phone: 203-737-2788; Fax: 203-737-1467; E-mail: peter.glazer@yale.edu

doi: 10.1158/1541-7786.MCR-15-0399

used yet more error-prone of the two pathways. Inherently, HR occurs only during S phase and early G_2 phase due to the necessity of a homologous template. In cancer, DSB repair is a priority, regardless of fidelity, to assure cell survival. As such, an even more mutagenic version of end joining, microhomology-mediated end joining (MMEJ), is often favored by tumors. MMEJ utilizes small nearby regions of homology to repair a break, always resulting in deletions. Although many mechanisms are likely involved in determining which DSB repair pathway to use, miRNAs may play an indirect role in regulating the activity of one pathway over the other to promote cell survival. miR-155 has been shown to be involved in the regulation of DSB repair factor, RAD51 (14), which identifies it as an important candidate for studying the role of miRNAs in modulating NHEJ and HR activity. In the context of miR-155 overexpression, the balance between HR and error-prone NHEJ has yet to be examined.

In addition to DSB repair, miR-155 also plays a role in other repair pathways. Mismatch repair deficiency due to miR-155 overexpression results in microsatellite instability *in vitro* (15). In addition, it has been shown that inflammation-induced expression of miR-155 leads to an increase in mutation frequency *in vitro* as measured by hypoxanthine phosphoribosyltransferase (HPRT) (16). Although this evidence is compelling, this phenomenon has yet to be explored *in vivo*, and the mechanism behind the observed increase in mutation is not fully understood. We set out to determine whether miR-155 overexpression *in vivo* results in genomic instability using a mouse model system. In addition, we hypothesized that other mechanisms beyond deficiency in mismatch repair might be responsible for the effect of miR-155 overexpression on genomic instability.

We report here that overexpression of miR-155 is sufficient to increase mutation frequency both in cells in culture and *in vivo* in a mouse model system. Upon overexpression of miR-155, we also find increased NHEJ activity and decreased HR activity, a pattern that is in keeping with an increase in mutation frequency based on the relative fidelity of these pathways. In addition to observing suppression of RAD51 and MLH1 in our system, we also analyzed global changes in mRNA levels by microarray in the presence of miR-155 overexpression to determine what other DNA repair mechanisms might be affected. We found that miR-155 overexpression leads to transcriptional repression of all four subunits of polymerase delta, a high-fidelity DNA repair polymerase. Interestingly, an established miR-155 target, FOXO3a, is a transcription factor with putative binding sites in the promoters of each of the four polymerase delta subunits, and we show that knocking down FOXO3a leads to a suppression of POLD1 expression at the protein level. Taken together, the results suggest that miR-155 downregulates polymerase delta by targeting the transcription factor FOXO3a, thereby inhibiting the transcription of the four polymerase delta subunits, resulting in an increased susceptibility to mutation by suppressing a high-fidelity polymerase and favoring error-prone translesion synthesis.

Materials and Methods

Cells

AV16 mouse epithelial cells harboring two mutation reporter transgenes, λ*supFG1* and *cII*, were derived as previously described in a C127 cell background (17). BICKO and 155KI mouse embryonic fibroblast (MEF) were derived from mice at embryonic day 13. AV16 cells were cultured in DMEM medium + 10% FBS + 0.8 mg/mL G418; BICKO MEF cells were cultured in DMEM medium + 15% FBS + 1× penicillin/streptomycin (pen/strep). The xrs6 Chinese hamster ovary cells are deficient in KU80 due to splice site mutation, and the xrs6+KU80 cells are derived from stable transfection of hamster wild-type XRCC5 cDNA (18). Both xrs6 and xrs6+KU80 cells were cultured in Ham's F12 medium + 10% FBS + 1× pen/strep. DLD1 and DLD1 *BRCA2*$^{-/-}$ (Horizon Discovery; HD 105-007) were cultured in McCoys 5A medium + 10% FBS + 1× pen/strep. *BRCA2*-deficient PEO1 and *BRCA2* proficient PEO1 C4-2 were gifts from T. Taniguchi (19) and were cultured in DMEM medium +10% FBS + 1× pen/strep. U20S EJ-DR cells, which have been previously described (20), contain the DR-GFP chromosomal reporter for HR and the EJ-RFP chromosomal reporter for mutagenic end-joining and were cultured in DMEM medium + 10% tetracycline-free FBS and 1× pen/strep. The U2OS DR-GFP cells have been previously described (21) and were cultured in DMEM medium + 15% FBS + 1× pen/strep. AV16, BICKO MEFs, and 155KI MEFs are all fibroblasts directly isolated from transgenic mice. The presence of the expected transgene or knock-in genotype was confirmed by PCR of genomic DNA. All other cell lines were obtained from Horizon Discovery (validation, SNP 6.0, and Sanger sequencing) or the ATCC (validation, cytochrome C oxidase I gene profiling, and short tandem repeat profiling).

In vitro miRNA overexpression

Human shMIMIC miRNA lentiviral particles expressing pre-miR-155 (155) or a nontargeting control (NTC) along with GFP were purchased from GE Dharmacon (originally VSH5841-10120825, miRIDIAN, and HMR5872; now VSH6185-202567165, SMARTchoice, and S-005000-01). Briefly, AV16 cells were transduced with lentiviral particles at 20 MOI for 48 hours, and pools were selected using puromycin after GFP expression appeared. Overexpression was confirmed by qRT-PCR.

Animals

miR-155 knock-in (*NesCre8; miR-155*^{LSLtTA}) mice (generously provided by Frank Slack, Yale University, New Haven, CT) were generated in a C57B6/129 hybrid background as previously described (9). Briefly, pre-miR-155 was cloned into the *ROSA26* locus behind a lox-stop-lox sequence along with a tTA, Tet-responsive element. This construct was used to generate a transgenic mouse model. Subsequently, these mice were crossed with *NesCre8* FVB/NJ mice to initiate miR-155 expression in the lymph and nervous system tissues, where Nestin-driven *Cre* is expressed (9). Breeding animals were kept on a doxycycline food diet to inhibit miR-155 expression in these tissues as it has been shown to induce a lymphoproliferative disease (9). *NesCre8; miR-155*^{LSLtTA}animals were crossed into another transgenic mouse line carrying the mutation reporter genes λ*supFG1* and *cII* as previously described (22, 23). The resulting animals (155KI) were genotyped for *NesCre8*, *miR-155*^{LSLtTA}, and λ*supFG1* as previously described (9, 24). 155KI and BICKO animals (ref. 25; provided by Frank Slack, Yale University, New Haven, CT) were utilized to generate MEFs.

Western blot

AV16 or BICKO cells were collected at 80% confluence by rinsing with PBS and scraping on ice. Protein was extracted using AZ lysis buffer (50 mmol/L Tris, pH 8, 250 mmol/L NaCl, 1% Igepal, 0.1% SDS, 5 mmol/L EDTA, 10 mmol/L $Na_4P_2O_7$, 10 mmol/L NaF) plus 1× protease inhibitor cocktail. Total protein (50 μg) was loaded and size fractionated on a 4% to 15% SDS-

polyacrylamide gel and transferred to a nitrocellulose membrane. Antibodies used were as follows: MLH1, RAD51, POLD1, FOXO3a, BRCA2, XRCC4, vinculin, β-actin, and tubulin. Antibodies were as follows: mouse monoclonal anti–α-tubulin (Sigma-Aldrich; 1:10,000; B-5-1-2); rabbit monoclonal anti-FOXO3a (Cell Signaling Technology; 1:1,000; 2497); rabbit polyclonal anti-RAD51 (Santa Cruz Biotechnology; 1:500; sc-8349); mouse monoclonal anti-MLH1 (BD Biosciences; 1:500; 554073); rabbit polyclonal anti-POLD1 (Santa Cruz Biotechnology; 1:200; sc-10784); mouse monoclonal anti–β-actin (Santa Cruz Biotechnology; 1:1,000; sc-47778); rabbit polyclonal anti-BRCA2 (Santa Cruz Biotechnology; 1:1,000; sc8326); mouse monoclonal anti-XRCC4 (BD Transduction Laboratories; 1:1,000; 611506); and mouse monoclonal anti-Vinculin (Abcam; 1:5,000; ab18058). Primary antibodies were incubated for 2 to 3 hours at room temperature or overnight at 4°C. Secondary goat-anti-mouse or goat-anti-rabbit antibodies (Thermo Fisher Scientific/Pierce) were used at a 1:5,000 dilution for 1 hour at room temperature. Primary and secondary antibodies were prepared in 5% milk. Tris Buffered Saline with Tween 20 washes were performed after primary incubation and after secondary incubation. Membranes were developed in SuperSignal West Pico Chemiluminescent Substrate (Thermo Fisher Scientific). Western blot quantification was performed using ImageJ software (NIH), comparing the intensity of the bands of interest with the intensity of loading controls. Values are reported as a fold change in intensity compared with the control sample, which is normalized to 1.

qRT-PCR

RNA was extracted from tissue culture or from organs of *NesCr8; miR-155*^{LSLtTA} mice using the mirVana miRNA Isolation Kit (Applied Biosystems/Life Technologies). Frozen organs were ground to a powder in liquid nitrogen and then lysed according to the manufacturer's protocol. cDNA was synthesized from total RNA using the Taqman miRNA High-Capacity cDNA Reverse Transcription Kit (Applied Biosystems/Life Technologies) with primers specific to hsa-miR-155, mmu-miR-155, and RNU6B or snoRNA202, endogenous controls for human or mouse, respectively. qRT-PCR was performed according to the manufacturer's protocol using the Taqman microRNA PCR system (Applied Biosystems/Life Technologies) as previously described (26). Briefly, cDNA was combined with Taqman Universal PCR Master Mix and Taqman probes specific for hsa-miR-155, mmu-miR-155, hsa-miR-128, and RNU6B or snoRNA202 (Applied Biosystems/Life Technologies). qRT-PCR was performed in 96-well optical plates. For analysis of POLD1, POLD2, POLD3, and POLD4 mRNA levels, RNA was extracted using the RNeasy Kit (Qiagen) with on column DNAse treatment. cDNA synthesis was carried out using the High-Capacity cDNA reverse transcriptase Kit (Applied Biosystems/Life Technologies). cDNA was combined with primers and Power SYBR Green PCR Master mix (Applied Biosystems/Life Technologies). Plates were spun down prior to analysis. miRNA C_t values were normalized to RNU6B or snoRNA202 Ct values, and relative expression was calculated using the $-\Delta\Delta$Ct method and reported with standard error for technical triplicate samples.

λ*supFG1* shuttle vector rescue and mutagenesis assay

High molecular weight DNA was isolated from organs or cells of interest and screened for mutation frequency as previously described (24). Briefly, DNA was isolated from spleens and brains of miR-155/Nestin-Cre knock-in animals using Phenol: Chloroform extraction. Isolated DNA was packaged into λ *in vitro* bacterial packaging extracts to rescue phage vectors. Packaging reactions were subsequently plated on Lysogeny Broth (LB) Agar or Terrific Broth Agar plates and incubated overnight at 37°C or 24°C, respectively, for λ*supFG1* or *cII* mutation analysis. Mutants were either screened by color (clear = mutants, blue = wild-type) or growth at 24°C for λ*supFG1* or *cII* mutation reporter genes, respectively. Mutation frequencies were determined based on the number of mutants identified per total number of plaques. A total of 50,000 plaques were screened per sample or animal. Statistical significance was determined using the unpaired *t* test (GraphPad Prism).

Mutant sequencing

Mutant plaques were isolated from LB Agar plates, PCR amplified using λ*supFG1* primers (23), purified, and sent to Yale's Keck Facility for sequencing. Mutation spectrum was determined based on the mutants identified by sequencing.

HR and NHEJ luciferase assays

The HR luciferase reporter, modeled after a similar assay described by the Samson lab (27), was constructed by cloning an inactivating I-SceI recognition site into the BstBI site 56 amino acids into the firefly luciferase gene in the gWIZ.Luciferase vector (Gelantis), and cloning a promoterless copy of the firefly luciferase open reading frame 700 base pairs downstream in reverse orientation as a donor template for HR. A DSB in the firefly luciferase gene was induced by I-SceI digestion and confirmed by electrophoresis. Linearized plasmid was transfected into cells to measure HR as a function of luciferase activity (firefly luciferase activity can only be restored by HR, which removes the inactivating I-SceI site). Renilla luciferase activity, expressed from pCMV-RL (Promega) transfected at a 1:20 ratio, was used as a transfection efficiency control. Forty-eight hours after transfection, luciferase activity from the HR reporter was normalized to gWIZ.Luciferase to calculate HR activity as percent reactivation.

The NHEJ luciferase assay is well characterized (28–32). Briefly, a HindIII-mediated DSB is induced between the promoter and the coding region of the firefly luciferase gene of pGL3 (Promega) and confirmed by electrophoresis. Linearized plasmid is transfected, and repair of this DSB by NHEJ restores firefly luciferase activity. NHEJ activity is determined by firefly luciferase activity measured 24 hours after transfection and normalized to a Renilla luciferase transfection control. Percent reactivation is determined by normalization of luciferase activity to the undamaged pGL3-Control vector. All luciferase reporter assays were performed in 12-well format by seeding 5×10^4 cells per well 24 hours before transfection and transfecting 1 μg of reporter or positive control vector and 50 ng Renilla luciferase vector per well. Luciferase activity was measured using the Dual Luciferase Reporter Assay System (Promega) for all samples. Statistical significance was determined by biologic triplicate.

Chromosomal GFP DSB reporter assays

U2OS DR-GFP reporter cell lines were transfected in triplicate with pre-miR-control (Ambion), pre-miR-155 (Ambion), or siRNA (BRCA2: Ambion s2085; RAD51: GE Dharmacon ON-TARGETplus SMART pool; XRCC4: GE:Dharmacon ON-TARGETplus SMART pool) to a final concentration of 20 nmol/L using an Amaxa Nucleofector (Lonza). SCE-I expression plasmid (4 μg) was transfected into 1×10^6 cells per replicate along with a second

dose of siRNA to a final concentration of 20 nmol/L 72 hours before analysis. Cells were analyzed for GFP expression by flow cytometry, and data were analyzed using the FlowJo software (Tree Star Inc.).

Mutagenic end-joining reporter assay

The mutagenic end-joining assay in the U2OS DR-EJ cells is well characterized, and reporter assays were carried out as previously described (20, 33). Briefly, U2OS DR-EJ cells were transfected to a final concentration of 20 nm with pre-miR-control (Ambion) or pre-miR-155 (Ambion) using the Amaxa Nucleofector (Lonza) in triplicate. Seventy-two hours after transfection, cells were exposed to media containing the Shield1 and triamcinolone acetonide ligands at concentrations of 1 μmol/L and 100 nmol/L, respectively, for 24 hours to induce a DSB in the RFP reporter. Seventy-two hours after the induction of the DSB, the percentage of RFP-positive cells was analyzed by flow cytometry, and data were analyzed using the FlowJo software (Tree Star Inc.). The data were normalized to the nontargeting pre-miR-control.

MMEJ host cell reactivation assays

Extrachromosomal MMEJ assays using pEJ2 (34) have been previously described (35). Briefly, pEJ2 was linearized with I-SceI digestion and transfected into 5×10^4 cells seeded 24 hours before transfection at a ratio of 1 μg per well. In parallel, cells were transfected using the same conditions with a positive control GFP expression vector pMAXGFP (Lonza) and a transfection efficiency control pDS-Red-Express-N1 (Clontech Laboratories). Fluorescence was quantified by flow cytometry 48 hours after transfection, and data were analyzed using FlowJo software (Tree Star Inc.) For each sample, GFP signal was normalized to RFP transfection efficiency and then normalized to the positive control to calculate percent reactivation. These cells were transfected in triplicate, and significance was calculated using an unpaired *t* test.

Microarray

RNA was isolated and purified from AV16 NTC or 155 or from BICKO$^{+/+}$ or BICKO$^{-/-}$ cells in biologic and technical triplicate using the RNeasy and QIAshredder kits (Qiagen). RNA was run on an Illumina MouseWG-6 V2 BeadChip Microarray Kit by the Yale Center for Genome Analysis. Analysis was performed to determine genes with expression changes greater than 20% with a *P* value of less than 0.01, which were depicted in a heat map.

siRNA knockdown

AV16 or U2OS-DR-GFP cells were seeded to 70% confluence. FOXO3a siRNA [GE Dharmacon; siGENOME mouse FOXO3 (56484) SMARTpool siRNA] was transfected using Dharmafect 1 (GE Dharmacon) at 100 nmol/L final concentration according to the manufacturer's protocol. BRCA2, RAD51, and XRCC4 siRNAs (BRCA2: Ambion s2085; RAD51: GE:Dharmacon ON-TARGETplus SMART pool; XRCC4: GE:Dharmacon ON-TARGETplus SMART pool) were transfected to a final concentration of 20 nmol/L accordingly using the Amaxa Nucleofector (Lonza) to the manufacturer's protocol. Cells were collected at several time points following transfection and processed for Western blot.

Comet assay

AV16 NTC, 155 BICKO+/+, or −/− cells were collected in the absence of treatment and examined by Comet assay (Trevigen) per the manufacturer's protocol, as previously described (36). Comet slides were electrophoresed for 45 minutes and imaged on an EVOS FL cell imaging microscope (Life Technologies). Comets were analyzed using CometScore software (TriTek Corp.), and at least 100 cells were scored for each sample. Data are presented as a mean of tail moment with standard error.

Results

miR-155 overexpression *in vitro* leads to an increase in mutation frequency

miR-155 overexpression has been shown to cause an increase in mutation frequency *in vitro* (16), but this phenomenon has yet to be examined *in vivo*. We decided to use a transgenic mouse reporter gene to assess the *in vivo* effect of miR-155 on mutagenesis in an animal model. To establish feasibility, we first tested for a detectable effect of miR-155 overexpression in cells in culture using the same reporter system as in the transgenic mice. For this, we generated a stable mouse cell line overexpressing miR-155 in a previously derived mouse epithelial cell line, AV16, carrying both *cII* and λ*supFG1* mutation reporter transgenes (17). Cells were infected with an shMIMIC lentiviral construct expressing pre-miR-155 (155) or an NTC. Cells incorporating the construct were selected and pooled by treatment with puromycin. Cells expressing the miR-155 construct had a significant increase in miR-155 expression as measured by qRT-PCR relative to NTC cells (Fig. 1A).

AV16 NTC and 155 cells were collected, DNA was isolated, and mutation frequency was analyzed to determine mutation frequency *in vitro*. Because the reporter genes are carried in a recoverable lambda phage-based shuttle vector, incubation of DNA with bacterial packaging extracts allowed for a temperature-dependent mutation screen in indicator bacteria. We determined that overexpression of pre-miR-155 in AV16 cells resulted in a 2-fold increase in mutation frequency relative to the AV16 NTC cells (Fig. 1B). This demonstrates that miR-155 overexpression drives an increase in mutation frequency in this reporter system.

Because several DNA repair factors have been identified as bona fide miR-155 targets, including HR facilitator RAD51 and mismatch repair factor MLH1, we set out to confirm their repression upon overexpression of miR-155 in the AV16 cells. Both of these targets were suppressed at the protein level by Western blot in this system (Fig. 1C), which could contribute to the observed increase in mutation frequency, in keeping with previous reports (15, 16).

miR-155 overexpression increases mutation frequency *in vivo*

Once miR-155–driven mutagenesis was confirmed in our *in vitro* system, we examined the role of miR-155 in maintaining genomic integrity *in vivo*. We utilized a conditional miR-155 knock-in mouse model. Briefly, a "tet-off" tTA-miR-155 sequence was cloned into the *Rosa26* locus behind a *loxP*-floxed stop cassette, and mice were generated in a B6 background. These mice, *miR-155*^{LSLtTA}, were crossed with a Nestin-driven Cre mouse model to generate a tetracycline-regulated Nestin-Cre *loxP* miR-155 knock-in mouse model (*NesCre8; miR-155*^{LSLtTA}; ref. 9). Nestin-Cre allows for spatially controlled expression of miR-155 in tissues where Nestin is constitutively expressed, which includes lymph and nervous system tissues. We crossed these animals with a transgenic mutation reporter mouse model (AV) carrying the *cII* and λ*supFG1* reporter genes (37). Resulting animals (155KI) were genotyped for *NesCre8*, *miR-155*^{LSLtTA}, and λ*supFG1* and were raised in the absence of doxycycline, enabling

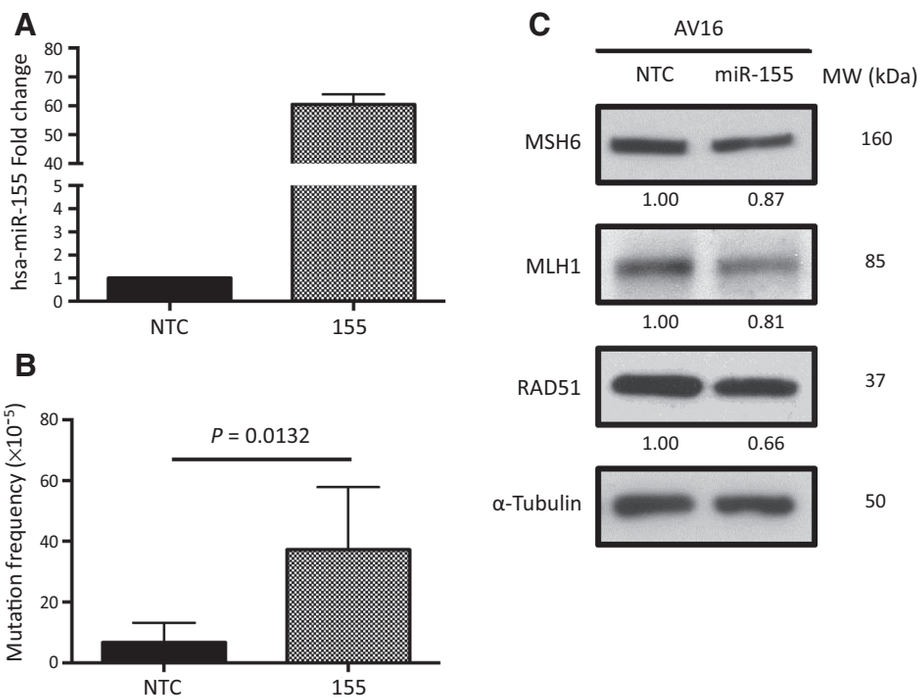

Figure 1.
miR-155 overexpression leads to an increase in mutation frequency *in vitro* and suppression of DNA repair factors. A, miR-155 overexpression in AV16 mouse epithelial cells by lentiviral infection is confirmed by qRT-PCR. B, mutation frequency is measured using a *cII* mutation reporter gene in the presence or absence of miR-155 overexpression. Error bars are calculated based on SEM and *P* value by unpaired *t* test ($n = 5$). C, RAD51, MLH1, and MSH6 Western blots measure translational repression by miR-155 overexpression. Quantifications are normalized to the NTC bands.

the overexpression of miR-155 in Nestin-expressing tissues. At 8 weeks of age, animals were sacrificed and tissues were harvested. This time point was chosen for humane reasons as these animals typically develop severely debilitating lymphoma beginning around 10 weeks of age (9).

To confirm miR-155 overexpression in specific organs, we isolated RNA from spleen and brain tissue of control (WT) or 155KI animals and analyzed miR-155 expression by qRT-PCR. As expected, both spleen and brain displayed significant overexpression of miR-155 (Fig. 2A and B), correlating with a *Nestin*-driven expression pattern. We chose to analyze the spleen due to the infiltration of lymphocytes, as previously reported, resulting in enlarged spleen size (Fig. 2C; ref. 9). The brain was chosen to confirm findings in another tissue in the absence of pathologic response to miR-155 overexpression.

To determine whether there was an *in vivo* effect on mutation frequency, we utilized a λ*supFG1* mutation reporter assay. DNA was isolated from spleen tissue as well as lymphadenopathy (tumor) tissue and analyzed for the frequency of mutation in the presence or absence of miR-155 overexpression. We utilized a blue/white bacterial plaque screen to quantify the mutation frequency in the λ*supFG1* gene. We found that 155KI mice had at least a 6-fold increase in mutation frequency in the spleen and representative tumors at the 8-week time point (Fig. 2D).

Importantly, we analyzed the mutation frequency in brain tissue as well, where *Nestin* is highly expressed, to test whether the increase in mutation frequency could be directly attributed to the overexpression of miR-155 and rather than a secondary mutagenic effect that might accompany the induced lymphomagenesis. Indeed, in brain tissue, where no significant pathology is observed (9), we detected a 2-fold increase in mutation frequency in 155KI mice when compared with controls (Fig. 2E). It is important to note that the baseline mutation frequency in the 8-week-old brain is roughly 5-fold higher than in the spleen. Additional work is necessary to conclusively determine the source of this difference; however, it is possible that due to the highly metabolic nature of the nervous tissue, a higher level of oxidative stress is observed, accounting for the difference in baseline mutation. In fact, it has been demonstrated that higher levels of oxidative base damage are observed at baseline in the rodent brain compared with the spleen (38–40). Nonetheless, these data suggest that the overexpression of miR-155 leads to increased mutagenesis *in vivo*.

We next evaluated whether the miR-155–induced mutations showed a pattern consistent with deficient mismatch repair. We analyzed the sequences of the mutations observed within the λ*supFG1* reporter gene. A hallmark of mismatch repair deficiency is an increase in single-nucleotide insertion/deletion mutations (22). In an analysis of λ*supFG1* gene mutations from spleen samples, we did not see a significant shift in mutation pattern between the control and 155KI spleen mutations (Supplementary Fig. S1), suggesting that suppression of another mechanism of DNA repair other than mismatch repair is likely playing a greater role in generating mutation than mismatch repair deficiency. This result is further supported by analysis of the miR-155–induced mutations in the *HPRT* gene *in vitro* observed by Croce and colleagues (16). It is important to note that the λ*supFG1* mutation assay is highly sensitive to mismatch repair deficiency and readily reports small insertion and deletion mutations (due to runs of G:C base pairs in the *supFG1* gene), but it will inherently underestimate the level of large deletion mutagenesis induced by DSBs because large deletions inactivate the λ shuttle vector and so

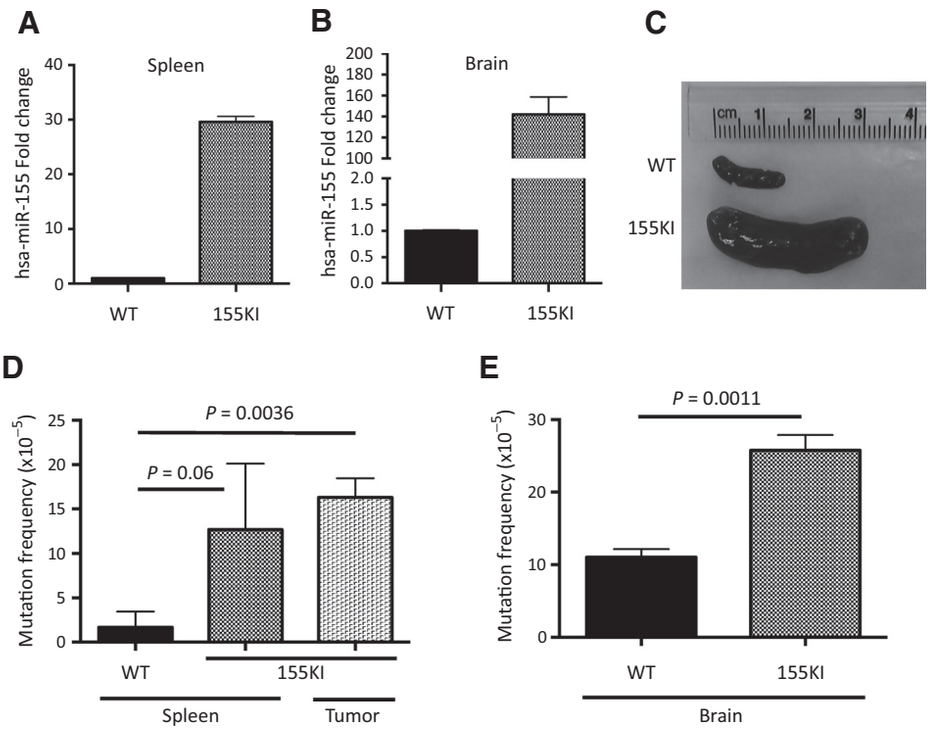

Figure 2.
miR-155 overexpression *in vivo* leads to an increase in mutation frequency. miR-155 overexpression was confirmed by qRT-PCR in the (A) spleen and (B) brain. C, representative images of spleens from WT and 155KI animals prior to DNA isolation. D, mutation frequency is measured by *supFG1* mutation reporter gene in the presence or absence of miR-155 overexpression in the spleen or in lymphadenopathy tissue (lymphoma), or (E) brain at 8 weeks of age. In both D and E, error bars are calculated based on SEM, and *P* value is calculated by unpaired *t* test (WT spleen: $n = 3$; 155KI spleen: $n = 4$; 155KI tumor: $n = 2$; WT brain: $n = 4$; 155KI brain: $n = 3$).

cannot be counted. Therefore, we analyzed DSBs by Comet assay as well, described later, to explore the hypothesis that miR-155 overexpression might be altering DSB repair and contributing to the observed increase in mutation.

miR-155 overexpression drives increased NHEJ activity and decreased HR activity

DSB repair can be divided into two main pathways, NHEJ and HR, both of which help to maintain genomic integrity. Pathway choice between HR and NHEJ is a complicated and not entirely understood process. NHEJ is the simpler of the two pathways and can take place in the absence of a homologous template, but it is also the more error-prone, occasionally resulting in deleterious mutations. Because miR-155 has been shown to target factors associated with DSB repair, we analyzed the level of baseline DSBs by neutral comet assay in AV16 155 cells compared with NTC cells. We found that overexpression of miR-155 resulted in a small, but statistically significant decrease in DSBs (Fig. 3A).

Conversely, to measure DSBs in the absence of miR-155, we examined the level of DSBs in a B-cell–induced cluster (BIC) knockout (BICKO) MEF cell line. BIC, also known as MIR155 host gene, is a gene that lacks an open reading frame and, as the name suggests, houses the primary miR-155 genomic sequence. BIC is transcribed by RNA polymerase II as a long noncoding RNA molecule that is ultimately processed into mature miR-155. In the absence of miR-155 expression, we found a significant increase in the level of DSBs at baseline (Fig. 3B). Importantly, we did not observe a change in the mutation frequency in the spleen when BICKO animals were crossed to the transgenic mutation reporter animals (data not shown), suggesting that although miR-155 loss seems to delay DNA repair or promote DSBs, this does not appear to lead to increased point mutagenesis. In addition, it suggests that the overexpression of miR-155 and the loss of miR-155 function act differently in modulating DSB repair. Taken together, these results suggest that tight regulation of miR-155 expression is necessary to maintain genomic integrity.

To determine whether these changes in DSB levels were due to a change in the efficiency of DSB repair, we utilized a panel of luciferase-based reporter assays engineered to score repair of DSBs through HR or NHEJ (Fig. 3C). In one assay, HR is measured based on restoration of luciferase expression following an I-SceI cut within a luciferase gene. A template copy of luciferase without a promoter for HR-based repair is located on the same plasmid. As a result, reactivation of luciferase activity provides a measure of HR activity. In the second assay, NHEJ activity is measured in a similar fashion except the HindIII site used to create a DSB is located between the promoter and the luciferase gene, and there is no homologous template within the plasmid. When the enzyme cuts, luciferase cannot be expressed, but if the DSB is repaired by NHEJ, expression is restored. Control matched pair cell lines reported as expected to validate these assays. Specifically, BRCA2 modulation did not show any effect on NHEJ reporter activity in the DLD1 or PEO1 matched pair cell lines (Supplementary Fig. S2A). In contrast, *BRCA2* knockout in DLD1 cells resulted in impaired HR reporter activity (Supplementary Fig. S2B), whereas *BRCA2* complementation in the PEO1 cells yielded a marked increase in HR activity (Supplementary Fig. S2B). Similarly, *Xrcc5* complementation of the xrs6 cell line did not induce changes in HR reporter activity (Supplementary Fig. S2B), but showed dramatic decreases in NHEJ reporter activity (Supplementary Fig. S2A). Taken together, these results demonstrate that these luciferase-based NHEJ and HR assays are reliable tools to analyze pathway-specific DNA repair across cell lines.

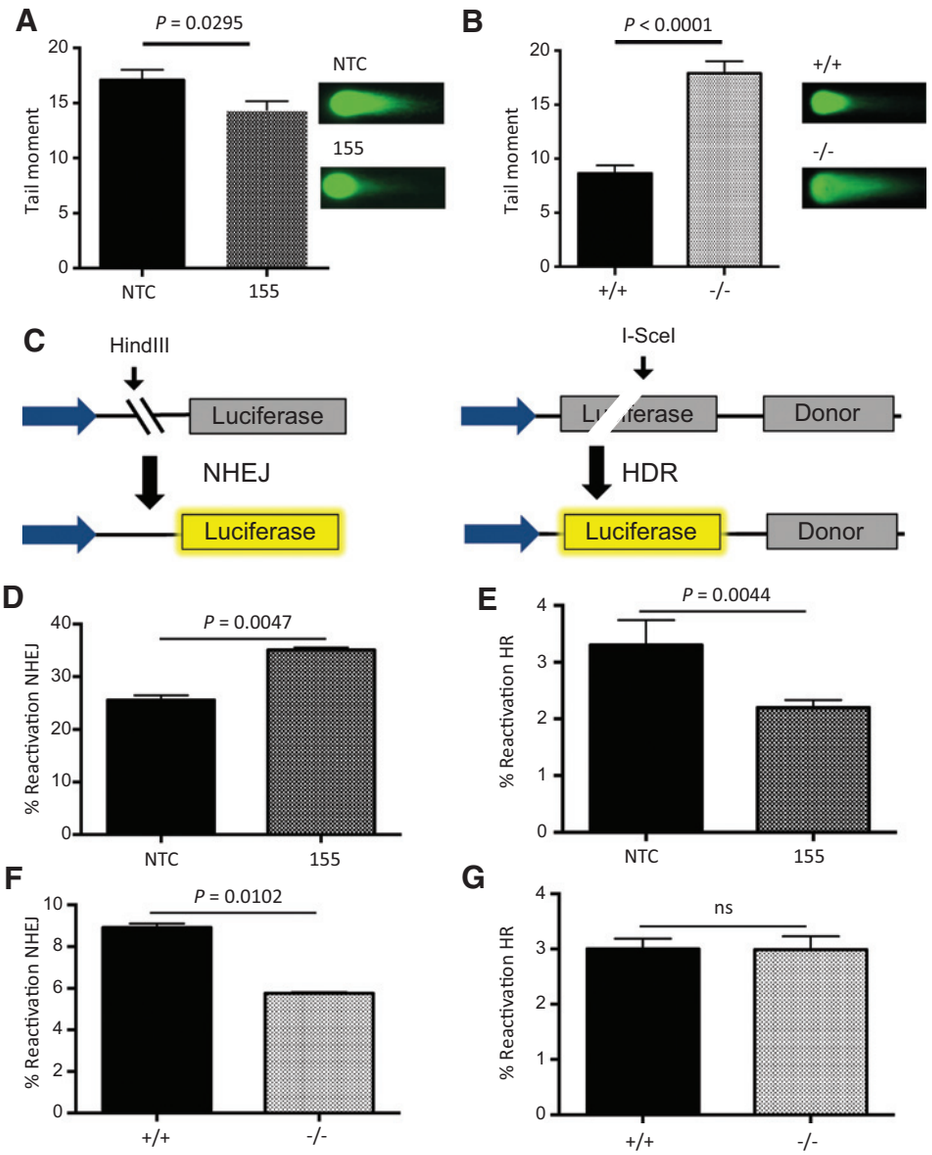

Figure 3.
DSB repair activity correlates with miR-155 expression. A, AV16 cells constitutively expressing NTC (black) or 155 (gray). B, MEFs either WT (black) or KO (gray) for the BIC locus containing the miR-155 gene were analyzed for DSBs using the neutral Comet assay. Error bars were calculated as SEM. *P* value was calculated by unpaired *t* test ($n = 3$). C, schematic representation of the luciferase reactivation assay measuring NHEJ or HR activity. NHEJ or HR luciferase reactivation was compared with a positive control to determine percent reactivation. A Renilla luciferase plasmid was used to control for transfection efficiency. D, AV16 NTC and 155 cells were analyzed for NHEJ and (E) HR activity using luciferase reactivation assays. MEFs WT or KO for miR-155 were analyzed for (F) NHEJ and (G) HR activity using the luciferase reactivation assays.

We found that AV16 155 cells show a decrease in HR when compared with the AV16 NTC cells as assayed by the luciferase HR reporter (Fig. 3D). We also measured HR activity using the U2OS-DR-GFP system. Validation of this system showed that BRCA2 and RAD51 knockdown (Supplementary Fig. S2C) demonstrated HR impairment (Supplementary Fig. S2D), whereas XRCC4 knockdown (Supplementary Fig. S2C) did not show any impairment in HR, as expected (Supplementary Fig. S2D). Similar to the luciferase HR assay, we observed a decrease in HR efficiency upon miR-155 overexpression by pre-miR-155 transfection, confirmed by FOXO3a repression (Supplementary Fig. S2C), in the U2OS DR-GFP cells (Supplementary Fig. S2D). In contrast, an increase in NHEJ was observed in AV16 155 cells when compared with the repair activity in AV16 NTC cells (Fig. 3E). The increase in NHEJ activity in the setting of miR-155 overexpression correlates with an observed decrease in unresolved DSBs but, because of the error prone nature of NHEJ, might also contribute to the observed increase in mutation frequency. To test this directly, we utilized the U2OS-DR-EJ cells (20) that contain an RFP reporter to measure total mutagenic end joining. Upon miR-155 overexpression, we observed an increase in mutagenic end joining as a function of miR-155 expression (Supplementary Fig. S2E). To further probe the mutagenic mechanism of miR-155, we examined the MMEJ pathway by host cell reactivation of the EJ2

Table 1. Relatively unchanged levels of NHEJ factors ($P > 0.05$)

Gene	Fold change (155 vs. NTC)	Fold change (KO vs. control)
Dclre1c	−1.03	−1.02
Dntt	−1.00	1.03
Lig4	1.03	1.07
Nhej1	1.02	1.03
Prkdc	1.01	1.00
Rad50	−1.01	1.02
Xrcc4	1.02	1.01
Xrcc5	−1.02	1.00
Xrcc6	−1.08	−1.05

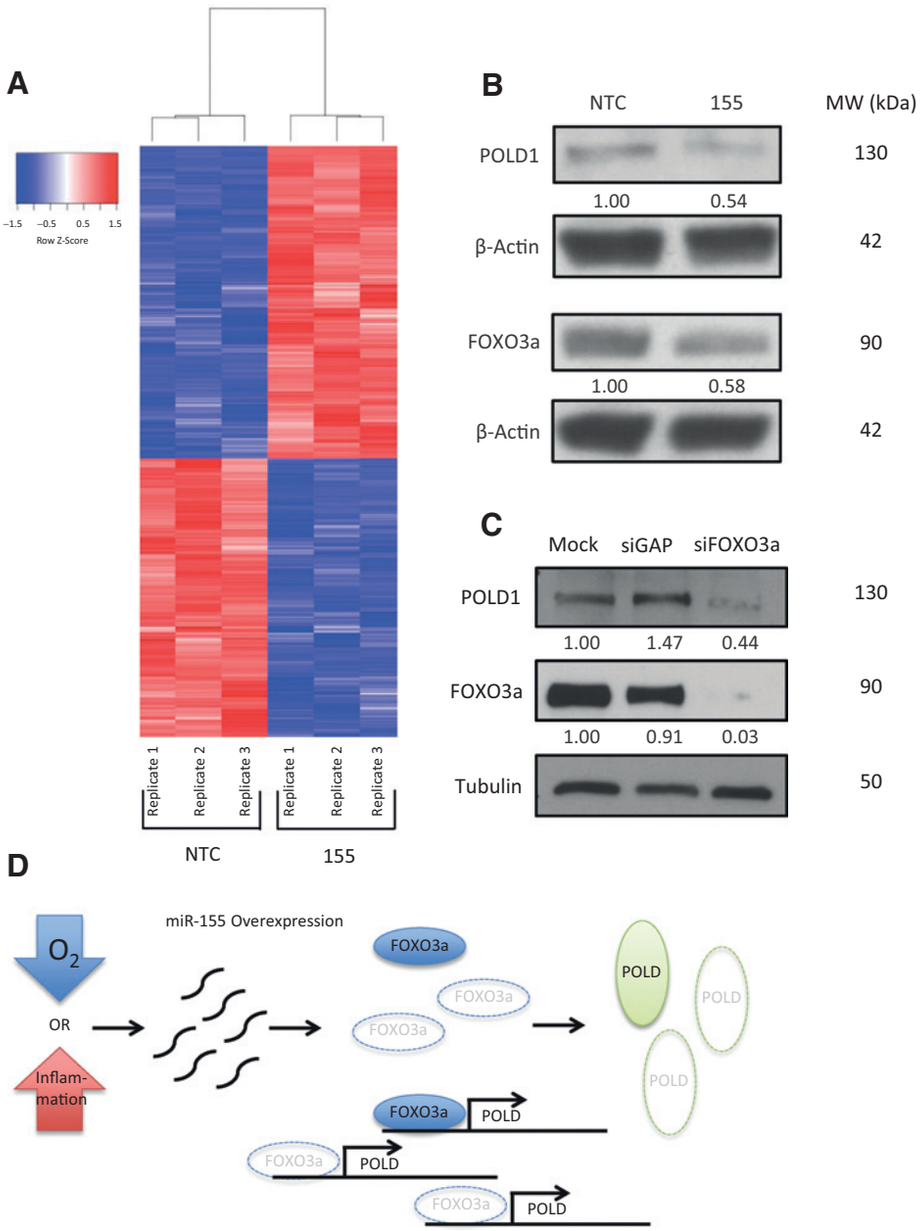

Figure 4.
Suppression of polymerase delta expression upon miR-155 overexpression is likely mediated by the FOXO3a transcription factor. A, microarray analysis reveals differential gene expression changes upon miR-155 overexpression. B, Western blot to analyze expression of FOXO3a and POLD1 in the presence of miR-155 overexpression in AV16 cells. C, siRNA knockdown of FOXO3a in AV16 cells and analysis of POLD1 expression by Western blot. D, schematic representation of miR-155 overexpression repressing FOXO3a expression and preventing FOXO3a from activating POLD expression, ultimately leading to an increase mutation frequency.

plasmid (34). To validate this assay, we analyzed the xrs6 cells compared with the xrs6 + KU80 cells and observed a decrease in MMEJ activity (Supplementary Fig. S2F), which is consistent with previous reports of KU80 suppressing MMEJ (34, 41–43). Using the EJ2 plasmid, we compared 155KI MEFs to their wild-type controls. However, we did not identify a change in MMEJ activity in this system with miR-155 overexpression (Supplementary Fig. S2G). Taken together, these results indicate that miR-155 overexpression induces a functional decrease in HR efficiency with a concurrent increase in NHEJ activity.

In contrast, when we examined the level of NHEJ in BICKO cells lacking any miR-155 expression, we found the opposite effect. In the absence of miR-155, NHEJ activity is reduced compared with wild-type function (Fig. 3F), whereas MMEJ activity is upregulated (Supplementary Fig. S2H) as likely a compensatory mechanism. With respect to HR, however, we did not observe a change in activity in the absence of miR-155 (Fig. 3G), suggesting that HR factors may already be expressed at a sufficient level in the setting of normal miR-155 expression and that the absence of miR-155 therefore does not yield any further functional increase in HR.

miR-155 overexpression results in a decrease in DNA polymerase delta expression

To further elucidate the role of miR-155 in NHEJ activity, we analyzed changes in mRNA expression upon miR-155 overexpression. We hypothesized that overexpression of miR-155 might lead to altered expression of an NHEJ factor to mediate the measured increase in activity. Using an Illumina mouse whole-genome beadchip microarray, we compared mRNA levels in AV16 155 cells to those in AV16 NTC. Surprisingly, we did not see a

difference in mRNA expression of any NHEJ repair factors on the array (Table 1); however, we did find nearly 1,200 genes with at least a 20% change in expression in cells overexpressing miR-155 compared with control cells (Fig. 4A). Most notably, we observed a decrease in all four subunits of polymerase delta mRNA in miR-155 overexpressing cells (Table 2) and validated these findings using qRT-PCR (Supplementary Fig. S3). Polymerase delta is a high-fidelity polymerase that functions in replication and DNA repair. None of the polymerase delta subunits are predicted targets of miR-155; however, each subunit has at least one putative binding site within its promoter for the transcription factor FOXO3a, an established target of miR-155. Importantly, we identified several established transcriptional targets of FOXO3a that were also downregulated in our microarray, consistent with a functional effect of FOXO3a repression by miR-155 (Table 3). To explore the possibility of FOXO3a regulating polymerase delta expression, we used Western blot analysis to examine levels of FOXO3a and POLD1, the catalytic subunit of polymerase delta, in AV16 155 cells compared with AV16 NTC cells. We found that both FOXO3a and POLD1 expressions are reduced in cells overexpressing miR-155 (Fig. 4B). In addition, we knocked down FOXO3a expression using siRNAs in the AV16 parent cells and found that POLD1 expression is subsequently reduced (Fig. 4C), but did not observe any effect on the NHEJ pathway (Supplementary Fig. S4). Taken together, these results suggest that miR-155 suppresses the expression of the transcription factor FOXO3a, subsequently reducing levels of polymerase delta (Fig. 4D).

Discussion

We have demonstrated that the overexpression of miR-155 is sufficient to drive an increase in mutation frequency both *in vitro* and *in vivo*. In addition, we confirmed prior reports that miR-155 overexpression mediates the repression of key DNA repair factors, MLH1 and RAD51, and we discovered that miR-155 suppresses the expression of all four subunits of the DNA polymerase, polymerase delta. Our data correlate with previously published work indicating that miR-155 is capable of targeting select mismatch repair factors and that its overexpression can increase the mutation rate *in vitro* in colon cancer cells (15, 16). However, our analysis of mutation patterns suggests that our observed increase in mutation frequency driven by miR-155 may not simply reflect a mismatch repair deficiency but rather that other mechanisms likely contribute to this observed mutagenesis.

We also explored the role of miR-155 in regulating HR activity. As mentioned, miR-155 targets RAD51, an important factor in HR. We found that as a result of miR-155 overexpression, HR activity is reduced. At the same time, we found that NHEJ displays an increase in activity. A relative increase in NHEJ in preference to HR is another possible explanation for the observed increase in mutation frequency as NHEJ is a more error-prone DSB repair pathway than is HR.

Table 2. Downregulated DSB repair genes ($P < 0.05$)

Gene	Fold change (155 vs. NTC)	*P* value (155 vs. NTC)
Pold4	−1.93	1.99653E−06
Pold3	−1.35	0.014425434
Pold1	−1.35	0.004880594
Fen1	−1.22	0.00420546
Mre11a	−1.17	0.004091406
Rpa2	−1.17	0.017108579
Rpa3	−1.16	0.019565474
Hus1	−1.16	0.000687722
Pold2	−1.14	0.057739236
Rad1	−1.14	0.000274311
Rad51	−1.13	0.004452602
Rad51C	−1.13	0.014211263
Poll	−1.11	0.022761465
Check2	−1.11	0.012247363

Table 3. Known FOXO3a targets downregulated upon miR-155 overexpression ($P < 0.05$)

Symbol	Fold change (155 vs. NTC)	*P* value (155 vs. NTC)
Bcl2l11	−1.31	0.001974636
Foxm1	−1.36	0.004424737
Gadd45a	−1.54	0.007134949

Upon further investigation, we discovered that overexpression of miR-155 also results in a decrease in polymerase delta mRNA and protein expression. This decrease correlates with suppression of FOXO3a, a transcription factor and known miR-155 target (1, 10, 44). Importantly, there are putative binding sites for FOXO3a within the promoter of all four subunits of polymerase delta, suggesting the possibility that FOXO3a may be involved in the regulation of polymerase delta expression. To confirm this hypothesis, we found that experimental suppression of FOXO3a by siRNA transfection results in a decrease in polymerase delta expression, demonstrating that the FOXO3a transcription factor promotes expression of polymerase delta. Although known FOXO3a targets are downregulated in our miR-155 overexpression system, we find that FOXM1, an oncogenic transcription factor that is typically upregulated upon FOXO3a repression (45), is downregulated. Despite seeming contradictory to the FOXO3a–FOXM1 axis in DNA repair and cancer (46), this suppression of FOXM1 might also contribute to genomic instability as FOXM1 has been shown to be an important mediator of genomic integrity. In fact, it has been suggested that repression of FOXM1 delays the G_2 phase of the cell cycle and can cause chromosomal instability (47). It is possible that a delay in the G_2 phase in the presence of functionally stunted HR and overactive NHEJ might further support the increased mutagenesis observed with miR-155 overexpression, although further studies are warranted to test this hypothesis.

Additional evidence supporting the relationship between miR-155, FOXO3a, and polymerase delta comes from phenotypic observations of transgenic mice. In fact, although *Pold1* knockout mice are embryonic lethal (48), *Foxo3* knock-out mice are viable and are prone to develop malignancies (49–51). Interestingly, the 155KI animals are also prone to malignancy, namely a lymphoma-like disorder, which has been previously reported (9). These observations support the hypothesis of a functional relationship between miR-155, FOXO3a, and polymerase delta.

Although direct experimental downregulation of polymerase delta has not been evaluated, several studies have shown that aberrant polymerase delta expression or function can cause increased levels of mutagenesis (48, 52–54). Therefore, the miR-155–mediated decrease in polymerase delta expression that we have observed is likely a key contributor to the increased genomic instability that is produced upon overexpression of miR-155. We hypothesize that compensation for a decrease in high-fidelity polymerase delta might involve the increased activity of other, more error-prone translesion polymerases, contributing to the observed increase in mutation frequency with miR-155 overexpression. It is tempting to speculate that previously reported

hypoxic induction of miR-155 (1) might promote genomic instability in hypoxia by the suppression of high-fidelity polymerase delta coupled with concurrent HIF1α-dependent overexpression of polymerase iota (55), a translesion polymerase. Another possibility is that reduced polymerase delta expression is compensated for by an increase in activity of polymerase theta, which mediates MMEJ (56, 57) and might contribute to an increase in mutation frequency. Both of these hypotheses will require further study.

MiRNAs are quickly being identified as key regulators of genomic stability, and understanding their function mechanistically as it relates to tumorigenesis will become a crucial part of personalized treatment. In addition to our evidence for the role of miR-155 in maintaining genomic integrity, a recent study demonstrated that three other miRNAs, miR-148b*, miR-193b*, and miR-1255b, play important roles in regulating the timing of HR to prevent LOH during the G_1 phase of the cell cycle (58). It is likely that several other miRNAs exist to regulate DNA repair pathways and ensure fidelity of the DNA damage response.

Elucidating the role of miR-155 in promoting tumorigenesis is an important step in developing adjuvant therapies to sensitize miR-155 overexpressing tumors to chemotherapeutic agents. As an oncomiR, miR-155 is an attractive target for personalized medicine. Importantly, miR-155 is not the first miRNA to be explored as a therapeutic target or agent. In fact, a phase IIa clinical trial using an anti–miR-122 agent has been positively evaluated as a treatment for Hepatitis C, and a phase I trial is ongoing using a miR-34 mimic to treat unresectable liver cancer (59, 60). Although further study is necessary to determine the effects of an antagomiR on preventing genomic instability, miR-155 is a promising target candidate for improving efficacy of current therapy, and our group is currently pursuing strategies to selectively inhibit miR-155 in tumors (61).

Disclosure of Potential Conflicts of Interest

No potential conflicts of interest were disclosed.

Authors' Contributions

Conception and design: J.R. Czochor, P.M. Glazer
Development of methodology: P. Sulkowski, P.M. Glazer
Acquisition of data (provided animals, acquired and managed patients, provided facilities, etc.): J.R. Czochor, P. Sulkowski
Analysis and interpretation of data (e.g., statistical analysis, biostatistics, computational analysis): J.R. Czochor, P. Sulkowski
Writing, review, and/or revision of the manuscript: J.R. Czochor, P. Sulkowski, P.M. Glazer
Administrative, technical, or material support (i.e., reporting or organizing data, constructing databases): P.M. Glazer
Study supervision: P.M. Glazer

Acknowledgments

The authors thank Denise Hegan for her technical assistance and Frank Slack for providing reagents.

Grant Support

This work was supported by NIH R01 ES005775 (to P.M. Glazer).

The costs of publication of this article were defrayed in part by the payment of page charges. This article must therefore be hereby marked *advertisement* in accordance with 18 U.S.C. Section 1734 solely to indicate this fact.

Received September 23, 2015; revised January 19, 2016; accepted January 28, 2016; published OnlineFirst February 5, 2016.

References

1. Babar IA, Czochor J, Steinmetz A, Weidhaas JB, Glazer PM, Slack FJ. Inhibition of hypoxia-induced miR-155 radiosensitizes hypoxic lung cancer cells. Cancer Biol Ther 2011;12:908–14.
2. Bruning U, Cerone L, Neufeld Z, Fitzpatrick SF, Cheong A, Scholz CC, et al. MicroRNA-155 promotes resolution of hypoxia-inducible factor 1alpha activity during prolonged hypoxia. Mol Cell Biol 2011;31:4087–96.
3. Papaconstantinou IG, Manta A, Gazouli M, Lyberopoulou A, Lykoudis PM, Polymeneas G, et al. Expression of microRNAs in patients with pancreatic cancer and its prognostic significance. Pancreas 2013;42:67–71.
4. Shibuya H, Iinuma H, Shimada R, Horiuchi A, Watanabe T. Clinicopathological and prognostic value of microRNA-21 and microRNA-155 in colorectal cancer. Oncology 2010;79:313–20.
5. Yanaihara N, Caplen N, Bowman E, Seike M, Kumamoto K, Yi M, et al. Unique microRNA molecular profiles in lung cancer diagnosis and prognosis. Cancer Cell 2006;9:189–98.
6. Iorio MV, Ferracin M, Liu CG, Veronese A, Spizzo R, Sabbioni S, et al. MicroRNA gene expression deregulation in human breast cancer. Cancer Res 2005;65:7065–70.
7. Lee EJ, Gusev Y, Jiang J, Nuovo GJ, Lerner MR, Frankel WL, et al. Expression profiling identifies microRNA signature in pancreatic cancer. Int J Cancer 2007;120:1046–54.
8. Eis PS, Tam W, Sun L, Chadburn A, Li Z, Gomez MF, et al. Accumulation of miR-155 and BIC RNA in human B cell lymphomas. Proc Natl Acad Sci U S A 2005;102:3627–32.
9. Babar IA, Cheng CJ, Booth CJ, Liang X, Weidhaas JB, Saltzman WM, et al. Nanoparticle-based therapy in an in vivo microRNA-155 (miR-155)-dependent mouse model of lymphoma. Proc Natl Acad Sci U S A 2012;109:E1695–704.
10. Kong W, He L, Coppola M, Guo J, Esposito NN, Coppola D, et al. MicroRNA-155 regulates cell survival, growth, and chemosensitivity by targeting FOXO3a in breast cancer. J Biol Chem 2010;285:17869–79.
11. O'Connell RM, Chaudhuri AA, Rao DS, Baltimore D. Inositol phosphatase SHIP1 is a primary target of miR-155. Proc Natl Acad Sci U S A 2009;106:7113–8.
12. Wang Y, Scheiber MN, Neumann C, Calin GA, Zhou D. MicroRNA regulation of ionizing radiation-induced premature senescence. Int J Radiat Oncol Biol Phys 2011;81:839–48.
13. Jiang S, Zhang HW, Lu MH, He XH, Li Y, Gu H, et al. MicroRNA-155 functions as an OncomiR in breast cancer by targeting the suppressor of cytokine signaling 1 gene. Cancer Res 2010;70:3119–27.
14. Gasparini P, Lovat F, Fassan M, Casadei L, Cascione L, Jacob NK, et al. Protective role of miR-155 in breast cancer through RAD51 targeting impairs homologous recombination after irradiation. Proc Natl Acad Sci U S A 2014;111:4536–41.
15. Valeri N, Gasparini P, Fabbri M, Braconi C, Veronese A, Lovat F, et al. Modulation of mismatch repair and genomic stability by miR-155. Proc Natl Acad Sci U S A 2010;107:6982–7.
16. Tili E, Michaille JJ, Wernicke D, Alder H, Costinean S, Volinia S, et al. Mutator activity induced by microRNA-155 (miR-155) links inflammation and cancer. Proc Natl Acad Sci U S A 2011;108:4908–13.
17. Rogers FA, Manoharan M, Rabinovitch P, Ward DC, Glazer PM. Peptide conjugates for chromosomal gene targeting by triplex-forming oligonucleotides. Nucleic Acids Res 2004;32:6595–604.
18. Singleton BK, Priestley A, Steingrimsdottir H, Gell D, Blunt T, Jackson SP, et al. Molecular and biochemical characterization of xrs mutants defective in Ku80. Mol Cell Biol 1997;17:1264–73.
19. Sakai W, Swisher EM, Jacquemont C, Chandramohan KV, Couch FJ, Langdon SP, et al. Functional restoration of BRCA2 protein by secondary BRCA2 mutations in BRCA2-mutated ovarian carcinoma. Cancer Res 2009;69:6381–6.
20. Bindra RS, Goglia AG, Jasin M, Powell SN. Development of an assay to measure mutagenic non-homologous end-joining repair activity in mammalian cells. Nucleic Acids Res 2013;41:e115.

21. Nakanishi K, Cavallo F, Brunet E, Jasin M. Homologous recombination assay for interstrand cross-link repair. Methods Mol Biol 2011;745:283–91.
22. Hegan DC, Narayanan L, Jirik FR, Edelmann W, Liskay RM, Glazer PM. Differing patterns of genetic instability in mice deficient in the mismatch repair genes Pms2, Mlh1, Msh2, Msh3 and Msh6. Carcinogenesis 2006; 27:2402–8.
23. Narayanan L, Fritzell JA, Baker SM, Liskay RM, Glazer PM. Elevated levels of mutation in multiple tissues of mice deficient in the DNA mismatch repair gene Pms2. Proc Natl Acad Sci U S A 1997;94:3122–7.
24. Leach EG, Gunther EJ, Yeasky TM, Gibson LH, Yang-Feng TL, Glazer PM. Frequent spontaneous deletions at a shuttle vector locus in transgenic mice. Mutagenesis 1996;11:49–56.
25. Thai TH, Calado DP, Casola S, Ansel KM, Xiao C, Xue Y, et al. Regulation of the germinal center response by microRNA-155. Science 2007;316:604–8.
26. Crosby ME, Kulshreshtha R, Ivan M, Glazer PM. MicroRNA regulation of DNA repair gene expression in hypoxic stress. Cancer Res 2009;69:1221–9.
27. Nagel ZD, Margulies CM, Chaim IA, McRee SK, Mazzucato P, Ahmad A, et al. Multiplexed DNA repair assays for multiple lesions and multiple doses via transcription inhibition and transcriptional mutagenesis. Proc Natl Acad Sci U S A 2014;111:E1823–32.
28. Bau DT, Fu YP, Chen ST, Cheng TC, Yu JC, Wu PE, et al. Breast cancer risk and the DNA double-strand break end-joining capacity of nonhomologous end-joining genes are affected by BRCA1. Cancer Res 2004; 64:5013–9.
29. Li YH, Wang X, Pan Y, Lee DH, Chowdhury D, Kimmelman AC. Inhibition of non-homologous end joining repair impairs pancreatic cancer growth and enhances radiation response. PLoS One 2012;7:e39588.
30. Sears CR, Turchi JJ. Complex cisplatin-double strand break (DSB) lesions directly impair cellular non-homologous end-joining (NHEJ) independent of downstream damage response (DDR) pathways. J Biol Chem 2012;287:24263–72.
31. Wang HC, Chou WC, Shieh SY, Shen CY. Ataxia telangiectasia mutated and checkpoint kinase 2 regulate BRCA1 to promote the fidelity of DNA end-joining. Cancer Res 2006;66:1391–400.
32. Zhong Q, Chen CF, Chen PL, Lee WH. BRCA1 facilitates microhomology-mediated end joining of DNA double strand breaks. J Biol Chem 2002;277: 28641–7.
33. Soong CP, Breuer GA, Hannon RA, Kim SD, Salem AF, Wang G, et al. Development of a novel method to create double-strand break repair fingerprints using next-generation sequencing. DNA Repair (Amst) 2015; 26:44–53.
34. Bennardo N, Cheng A, Huang N, Stark JM. Alternative-NHEJ is a mechanistically distinct pathway of mammalian chromosome break repair. PLoS Genet 2008;4:e1000110.
35. Fattah FJ, Kweon J, Wang Y, Lee EH, Kan Y, Lichter N, et al. A role for XLF in DNA repair and recombination in human somatic cells. DNA Repair (Amst) 2014;15:39–53.
36. Kaushik Tiwari M, Rogers FA. XPD-dependent activation of apoptosis in response to triplex-induced DNA damage. Nucleic Acids Res 2013;41: 8979–94.
37. Rogers FA, Lin SS, Hegan DC, Krause DS, Glazer PM. Targeted gene modification of hematopoietic progenitor cells in mice following systemic administration of a PNA-peptide conjugate. Mol Ther 2012;20:109–18.
38. Hirano T, Yamaguchi R, Asami S, Iwamoto N, Kasai H. 8-hydroxyguanine levels in nuclear DNA and its repair activity in rat organs associated with age. J Gerontol A Biol Sci Med Sci 1996;51:B303–7.
39. Russo MT, De Luca G, Degan P, Bignami M. Different DNA repair strategies to combat the threat from 8-oxoguanine. Mutat Res 2007;614:69–76.
40. Russo MT, De Luca G, Degan P, Parlanti E, Dogliotti E, Barnes DE, et al. Accumulation of the oxidative base lesion 8-hydroxyguanine in DNA of tumor-prone mice defective in both the Myh and Ogg1 DNA glycosylases. Cancer Res 2004;64:4411–4.
41. McVey M, Lee SE. MMEJ repair of double-strand breaks (director's cut): deleted sequences and alternative endings. Trends Genet 2008;24:529–38.
42. Nussenzweig A, Nussenzweig MC. A backup DNA repair pathway moves to the forefront. Cell 2007;131:223–5.
43. Truong LN, Li Y, Shi LZ, Hwang PY, He J, Wang H, et al. Microhomology-mediated End Joining and Homologous Recombination share the initial end resection step to repair DNA double-strand breaks in mammalian cells. Proc Natl Acad Sci U S A 2013;110:7720–5.
44. Ling N, Gu J, Lei Z, Li M, Zhao J, Zhang HT, et al. microRNA-155 regulates cell proliferation and invasion by targeting FOXO3a in glioma. Oncol Rep 2013;30:2111–8.
45. McGovern UB, Francis RE, Peck B, Guest SK, Wang J, Myatt SS, et al. Gefitinib (Iressa) represses FOXM1 expression via FOXO3a in breast cancer. Mol Cancer Ther 2009;8:582–91.
46. Gomes AR, Zhao F, Lam EW. Role and regulation of the forkhead transcription factors FOXO3a and FOXM1 in carcinogenesis and drug resistance. Chin J Cancer 2013;32:365–70.
47. Laoukili J, Kooistra MR, Brás A, Kauw J, Kerkhoven RM, Morrison A, et al. FoxM1 is required for execution of the mitotic programme and chromosome stability. Nat Cell Biol 2005;7:126–36.
48. Uchimura A, Hidaka Y, Hirabayashi T, Hirabayashi M, Yagi T. DNA polymerase delta is required for early mammalian embryogenesis. PLoS One 2009;4:e4184.
49. Castrillon DH, Miao L, Kollipara R, Horner JW, DePinho RA. Suppression of ovarian follicle activation in mice by the transcription factor Foxo3a. Science 2003;301:215–8.
50. Paik JH, Kollipara R, Chu G, Ji H, Xiao Y, Ding Z, et al. FoxOs are lineage-restricted redundant tumor suppressors and regulate endothelial cell homeostasis. Cell 2007;128:309–23.
51. Tothova Z, Kollipara R, Huntly BJ, Lee BH, Castrillon DH, Cullen DE, et al. FoxOs are critical mediators of hematopoietic stem cell resistance to physiologic oxidative stress. Cell 2007;128:325–39.
52. Albertson TM, Ogawa M, Bugni JM, Hays LE, Chen Y, Wang Y, et al. DNA polymerase epsilon and delta proofreading suppress discrete mutator and cancer phenotypes in mice. Proc Natl Acad Sci U S A 2009;106:17101–4.
53. Goldsby RE, Hays LE, Chen X, Olmsted EA, Slayton WB, Spangrude GJ, et al. High incidence of epithelial cancers in mice deficient for DNA polymerase delta proofreading. Proc Natl Acad Sci U S A 2002;99:15560–5.
54. Venkatesan RN, Hsu JJ, Lawrence NA, Preston BD, Loeb LA. Mutator phenotypes caused by substitution at a conserved motif A residue in eukaryotic DNA polymerase delta. J Biol Chem 2006;281:4486–94.
55. Ito A, Koshikawa N, Mochizuki S, Omura K, Takenaga K. Hypoxia-inducible factor-1 mediates the expression of DNA polymerase iota in human tumor cells. Biochem Biophys Res Commun 2006;351:306–11.
56. Ceccaldi R, Liu JC, Amunugama R, Hajdu I, Primack B, Petalcorin MI, et al. Homologous-recombination-deficient tumours are dependent on Poltheta-mediated repair. Nature 2015;518:258–62.
57. Kent T, Chandramouly G, McDevitt SM, Ozdemir AY, Pomerantz RT. Mechanism of microhomology-mediated end-joining promoted by human DNA polymerase theta. Nat Struct Mol Biol 2015;22:230–7.
58. Choi YE, Pan Y, Park E, Konstantinopoulos P, De S, D'Andrea A, et al. MicroRNAs down-regulate homologous recombination in the G1 phase of cycling cells to maintain genomic stability. Elife 2014;3:e02445.
59. Janssen HL, Reesink HW, Lawitz EJ, Zeuzem S, Rodriguez-Torres M, Patel K, et al. Treatment of HCV infection by targeting microRNA. N Engl J Med 2013;368:1685–94.
60. Shibata C, Otsuka M, Kishikawa T, Yoshikawa T, Ohno M, Takata A, et al. et al.Current status of miRNA-targeting therapeutics and preclinical studies against gastroenterological carcinoma. Mol Cell Ther 2013;1:5.
61. Cheng CJ, Bahal R, Babar IA, Pincus Z, Barrera F, Liu C, et al. MicroRNA silencing for cancer therapy targeted to the tumour microenvironment. Nature 2015;518:107–10.